Fire-induced Winds in the 20 October 1991 Oakland Hills Fire

JAVIER TRELLES[1] and PATRICK J. PAGNI
Mechanical Engineering Department
University of California
Berkeley, CA 97420-1740, USA

ABSTRACT

The winds generated at 11:45 a.m. by 38 fires and at 12:00 p.m. by 259 fires for the 20 October 1991 Oakland Hills Fire are simulated using the Baum and McCaffrey mass fire model. Each house is modeled as having a 50 MW heat release rate at the time of the computation. For each single fire, the flame tip is 15 m high, the maximum vertical velocity is 16 m/s and the maximum radial velocity is 2.4 m/s. At 11:45 a.m., for the mass fire the maximum induced wind is 2.6 m/s. The maximum vertical velocity is 14 m/s. At 12:00 p.m., the maximum horizontal velocity is 13 m/s. The maximum vertical velocity is 26 m/s. Results indicate that the strong fire-induced winds at and after 12:00 p.m. contributed to the post-noon decrease in the fire spread rate in the ambient windward direction.

KEY WORDS: urban/wildland interface or intermix, fire-induced winds, mass fire modeling.

NOTATION

Roman

c_p	Specific heat (J/kg·K)
$\mathcal{D}/\mathcal{D}t$	Scalar operator $\partial/\partial t + \boldsymbol{u}\cdot\nabla$ (s^{-1})
$\hat{e}_j$	Unit vector in the j-direction
g	Acceleration of gravity (m/s^2)
h	Hypotenuse (m)
k	Thermal conductivity (W/m·K)
L_c	Characteristic length (m)
N	Number of fires/sources
p	Pressure (Pa)
$\dot{Q}_o$	Net total chemical heat release rate (W)

Greek

Θ^*	Dimensionless temperature difference
ρ	Density (kg/m^3)
Φ	Potential function (m^2/s)
Ψ	Stokes stream function (m^3/s)
ω	Vorticity (s^{-1})
∇	Gradient (del) operator, $\hat{e}_x\partial/\partial x + \hat{e}_y\partial/\partial y + \hat{e}_z\partial/\partial z$ (m^{-1})

Superscripts

*	Nondimensional quantity
·	Quantity per unit time
'''	Quantity per unit volume

1. Present address: Building and Fire Research Laboratory, National Institute of Standards and Technology, Bldg. 224, Rm. A345, Gaithersburg, MD 20889, USA.

NOTATION

$\dot{q}'''$	Total chemical power output (W/m^3)
R	Radius of Gaussian profile (m)
R_f	Fit for the width of the Gaussian profile (m)
r	Radial direction (m)
T	Temperature (K)
t	Time (s)
U, u	Velocity (m/s)
v^*, w^*	Solenoidal and expansion velocity vectors
X, Y, Z	1st, 2nd, and 3rd cartesian coordinates (m)
z	Axial direction (m)

Subscripts

c	Characteristic quantity
cl	Center-line quantity
i, j	Indices
o	Ambient condition
r	Radial component
X	X-direction component
Y	Y-direction component
Z	Z-direction component
z	Axial component

INTRODUCTION

On Saturday, 19 October 1991, the Oakland Fire Department responded to calls regarding a brush fire between Buckingham Boulevard and Marlborough Terrace. Saturday's weather was characteristic for the season: moderate onshore wind during the day, less intense offshore wind at the night. The temperature was hot (> 25° C) but the relative humidity was above 30% and the ambient winds were on the order of 3 m/s [1]. By the evening, the fire department was confident that the fire was out and that the ground was thoroughly soaked. Hose lines were left in place and fire companies were asked to check the burn area overnight [2,3].

On October 20, at 6:00 a.m., the normal weather pattern was interrupted as winds in excess of 10 m/s arose from N 35° E and the relative humidity dropped below 10%. These conditions prevailed until 5 p.m. This strong, dry convective current began to dramatically lower the moisture level of the previously soaked burn area. It also served to further desiccate brush and trees killed by the unusual freeze of January, 1991. The ambient temperature climbed to 32° C. The few embers that remained buried overnight were by 10:45 a.m. spotting to new areas of dry fuel. Between 11:15 and 11:30 a.m., extremely rapid fire spread in the windward direction overwhelmed the capabilities of the four-alarm crews called to help at 11:15. The swift growth continued until noon. From then on, the fire spread in the windward direction was not as fast, as is shown in Figs. 1 and 2. The initial brand material came primarily from Monterey pine, *Pinus radiata*. About 650 m from the fire origin, the fire engaged a 35 m high stand of *Eucalyptus globulus* [1] which quickly became an inferno releasing copious brands. Once structures became involved, the shakes and shingles they liberated further exacerbated the flaming brand problem.

The toll from this disaster was high. Twenty-five people lost their lives. 2,334 structures (3,469 living units) were destroyed. The estimated cost exceeds $1.5 billion. Six million m^2 (~ 1,500 acres) of area were affected within an approximate fire perimeter of 8.8 km. The area has remained scarred for years [1-4].

The purpose of this paper is to calculate, using the Baum and McCaffrey [5] mass fire model, the fire-induced winds and determine the effect of these winds on the observed fire

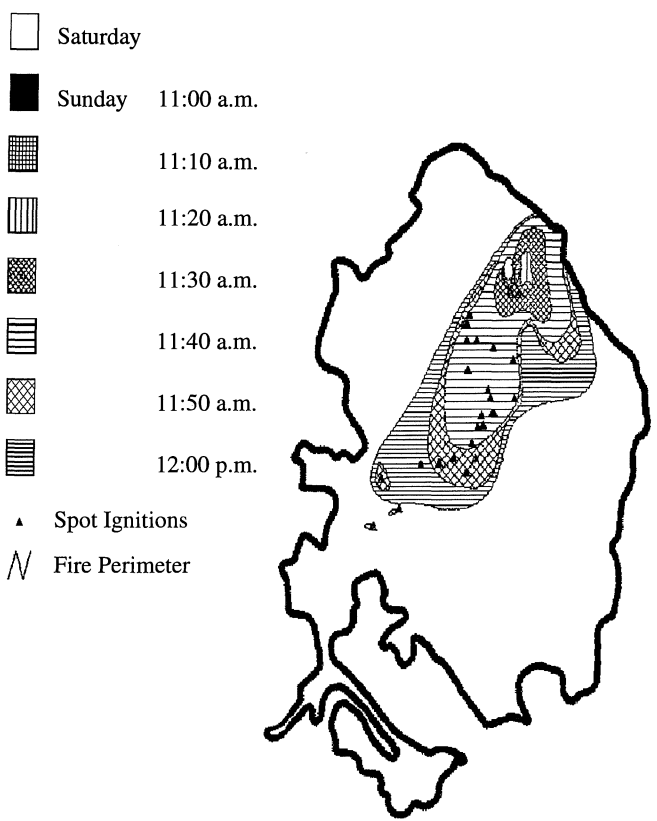

FIGURE 1: The fire spread between 11:00 a.m. and noon was rapid. The triangles represent spotting points determined from videos, official reports, and eyewitness accounts. Fire brand transport distances were most pronounced in the windward direction.

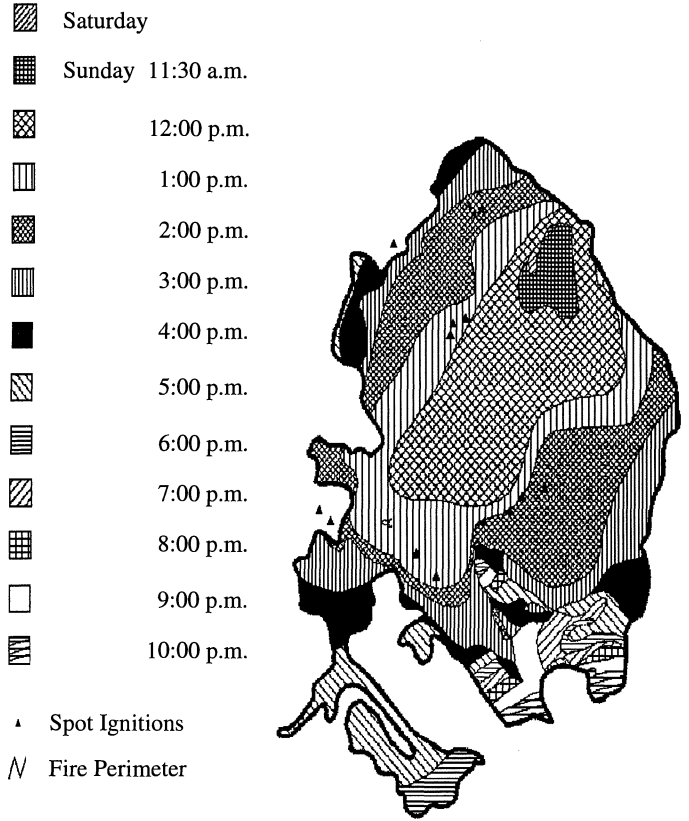

FIGURE 2: After noon, spotting in the windward direction was not as dramatic as before. The fire eventually burned 6 million square meters of area bounded by an 8.8 km perimeter.

spread. In particular, can the model explain why the wind-driven fire spread slowed significantly at noon, as shown in Fig. 2?

OBSERVATIONS

After the fire, the coordinates of burned structures were incorporated into a Graphical Information System (GIS) study using the Global Position System (GPS) [6]. These data provided points for placing model fires, as is shown in Figs. 3 and 4, within the official California Coordinate System which is in feet. The fire domain is bounded by X = [1,497,000 , 1,507,000] ft and Y = [491,000 , 503,000] ft. The origin is in the Pacific Ocean. The increasing Y-direction is north and the increasing X-direction is east. It is divided into 120 square sectors of equal area whose side lengths are 305 m (1000 ft). Different GIS layers can be employed to display terrain contours, property plots, vegetative content, etc. Of special interest is the sub-domain bounded by X = [1,501,000 , 1,507,000] ft and Y = [495,000 , 503,000] ft. This region, affected from 11:00 a.m. to 12:00 p.m., is the early-time study area focused on here.

The time contours shown in Figs. 1 and 2 are the bounding limits for spot fires [6]. A 15 minute delay was assumed for full involvement of the structures within the contours. So the 11:45 a.m. and noon house fires shown as dotted circles in Figs. 3 and 4 correspond respectively to the 11:30 and 11:45 a.m. contours in Figs. 1 and 2. In order to estimate the terrain-guided ambient wind in the early study area, Professor John Monteverdi, Chair of the Geosciences Department at San Francisco State University, was consulted [7]. He used wind measurements from local weather stations along with terrain data from the GIS data base to arrive at the estimated local ambient winds shown in Figs. 3 and 4 as light gray vectors.

The assumed heat release rate for an involved structure is shown in Fig. 5. It is convenient to replace the exponential profile with three constant steps: a peak burn rate of 45 MW for an hour, a moderate die down depicted as burning at 10 MW for three hours, and a final die down of 5 MW for three more hours, yielding extinction after an average total of 7 hours. The vegetation around the structure is estimated to contribute another 5 MW, resulting in the 50 MW plateau shown in Fig. 5 which is used as a constant heat release rate pool fire model for a typical burning structure. Multiple, connected structures, such as condominium townhouses, were approximated as 30 MW for each unit. A condominium fire's strength and location is therefore based on the centroid of the townhouses in the smallest grouping which is continuous. The configurations that existed here were not so long that a line fire model was required.

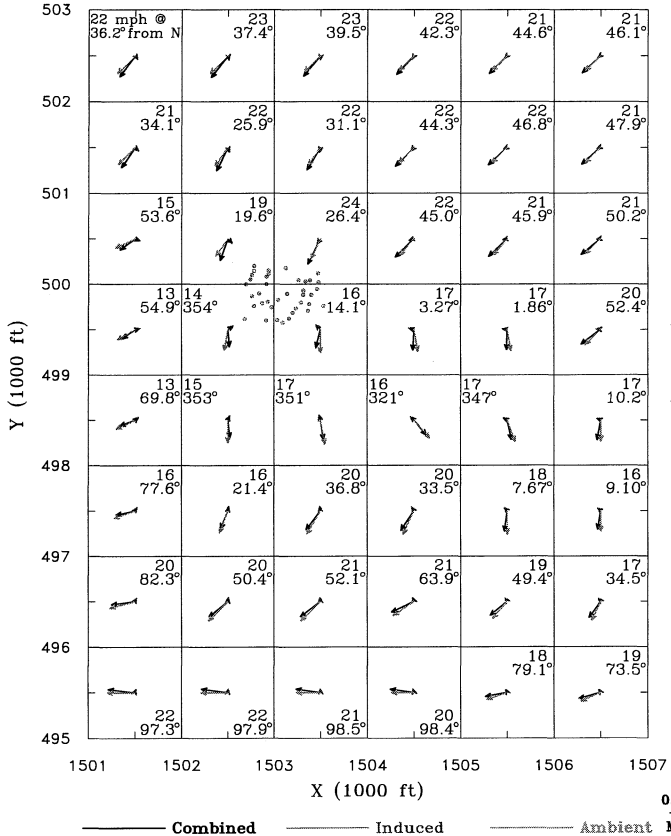

FIGURE 3: Horizontal induced winds @ 20 m, 1145 a.m. ± 5 min. The dotted circles indicate all 38 of the 50 MW fires that are driving the flow. So few fires barely affect the prevailing wind.

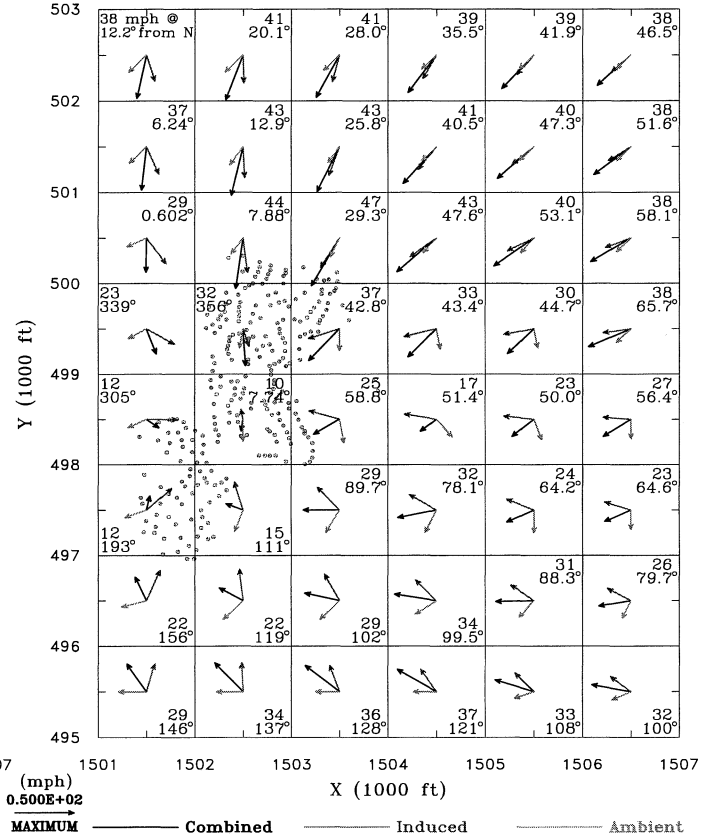

FIGURE 4: Horizontal combined winds @ 20 m, 1200 p.m. ± 10 min. 259 fires are burning at rates which vary from 50 to 330 MW. Now that the fire has grown in strength, the magnitude of the fire-induced winds is comparable to that of the ambient.

MODELING

The following approximate plume equations have been derived [8] from the general turbulent combustion equations:

$$\text{Continuity:} \qquad \frac{\partial \rho}{\partial t} + \boldsymbol{u} \cdot \nabla \rho + \rho(\nabla \cdot \boldsymbol{u}) = 0,$$

$$\text{Momentum:} \qquad \rho \frac{\partial \boldsymbol{u}}{\partial t} + \rho \boldsymbol{u} \cdot \nabla \boldsymbol{u} = -\nabla \tilde{p} + (\rho - \rho_o) g \hat{\boldsymbol{e}}_z, \tag{1}$$

$$\text{Energy:} \qquad \rho c_p \left(\frac{\partial T}{\partial t} + \boldsymbol{u} \cdot \nabla T \right) = \dot{q}'''.$$

where axisymmetry is assumed. The boundary conditions at infinity are $\boldsymbol{u} = \boldsymbol{0}$, $\rho = \rho_o$, $T = T_o$, and the ambient pressure perturbation is $\tilde{p} = 0$. Define the following dimensionless variables:

$$t^* = t/t_c; \qquad \rho^* = \rho/\rho_o; \qquad T^* = T/T_o;$$
$$\nabla^* = L_c \nabla; \qquad \tilde{p}^* = \tilde{p}/p_c; \qquad u^* = u/U_c; \qquad \text{and} \qquad \dot{q}'''^* = \dot{q}''' L_c^3/\dot{Q}_o. \tag{2}$$

where $\dot{Q}_o$ is the specified fire heat release rate. Substituting Eqs. (2) in Eqs. (1) gives

$$\frac{\partial \rho^*}{\partial t^*} + \frac{U_c t_c}{L_c} (\boldsymbol{u}^* \cdot \nabla^* \rho^* + \rho^* (\nabla^* \cdot \boldsymbol{u}^*)) = 0, \tag{3}$$

from which $U_c = L_c/t_c$. The momentum equation then becomes

$$\rho^* \left(\frac{\partial \boldsymbol{u}^*}{\partial t^*} + \boldsymbol{u}^* \cdot \nabla^* \boldsymbol{u}^* \right) = -\frac{p_c t_c^2}{\rho_o L_c^2} \nabla^* p^* + \frac{g t_c^2}{L_c} (\rho^* - 1) \hat{e}_z, \tag{4}$$

which gives $t_c = (L_c/g)^{1/2}$ and $p_c = \rho_o g L_c$. The energy equation is

$$\rho^* \left(\frac{\partial T^*}{\partial t^*} + \boldsymbol{u}^* \cdot \nabla^* T^* \right) = \dot{q}'''^* \frac{\dot{Q}_o t_c}{\rho_o c_p T_o L_c^3}, \tag{5}$$

from which $\dot{Q}_o t_c/(\rho_o c_p T_o L_c^3) = 1$. Substituting for t_c and solving for L_c allows the determination of the characteristic length, time, and velocity as

$$L_c \equiv \left(\frac{\dot{Q}_o}{\rho_o c_p T_o \sqrt{g}} \right)^{2/5}, \qquad t_c \equiv \left(\frac{\dot{Q}_o}{g^3 \rho_o c_p T_o} \right)^{1/5}, \qquad \text{and} \qquad U_c \equiv \left(\frac{g^2 \dot{Q}_o}{\rho_o c_p T_o} \right)^{1/5}. \tag{6}$$

The nondimensional equation of state is $\rho^* T^* = 1$ since ρT is assumed constant. The nondimensional equations governing plumes are then

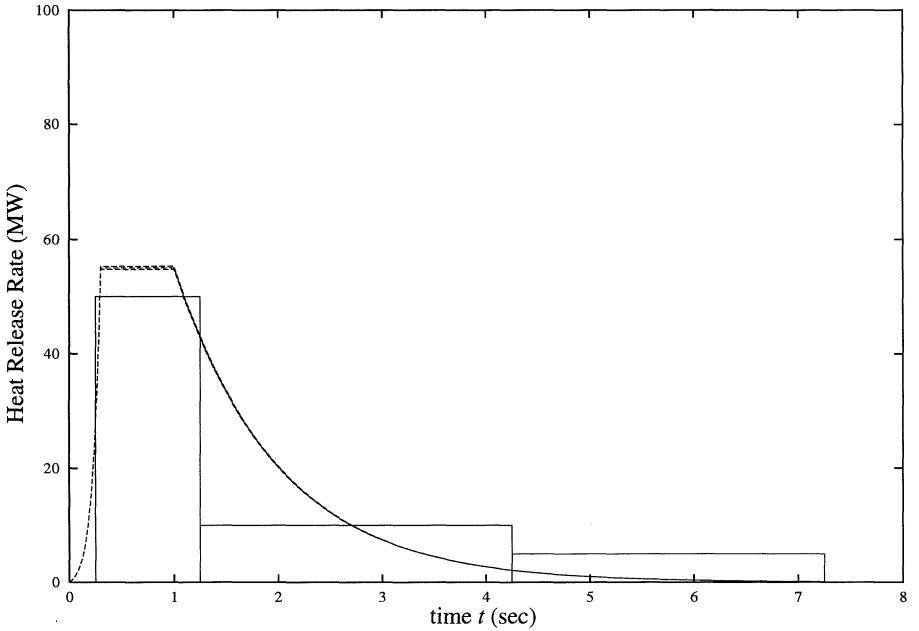

FIGURE 5: The typical heating rate for an involved house yields, in the absence of vegetation, a total energy of 90 MW·hrs. The fire grows exponentially, burns at a maximum for about an hour, then exponentially dies out. The rectangles are useful approximations to this history. In this simplified representation, a house will be at a peak burn rate of 45 MW for an hour. The vegetation around the structure is estimated to contribute 5 MW, resulting in the 50 MW shown in the figure. The die down is depicted as burning at 10 MW for three hours followed by 5 MW for three more hours and finally extinction after an average total of 7 hours.

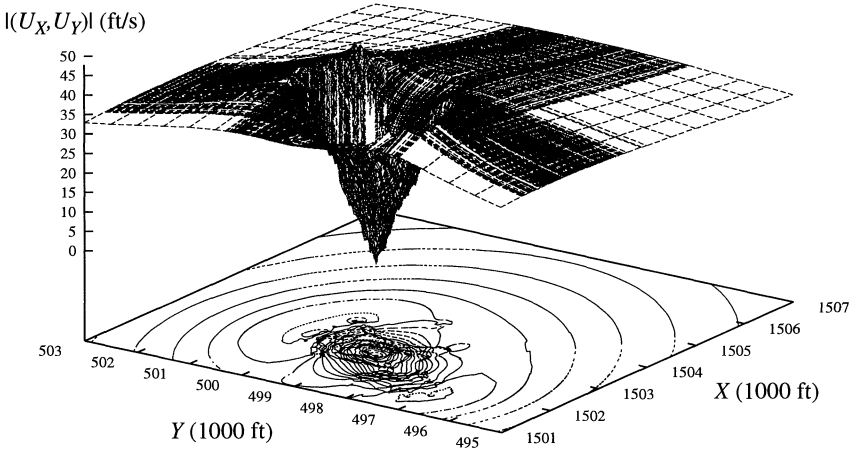

FIGURE 6: The magnitude of the 12:00 p.m. horizontal inflow velocities at 30 m altitude are shown here as contours and as a 3-D surface. A grid based on the X-Y location of the 259 fires is superimposed on the uniform grid in order to resolve the complex behavior near the sources.

$$\text{Continuity:} \qquad \frac{\partial \rho^*}{\partial t^*} + (\boldsymbol{u}^* \cdot \nabla^* \rho^* + \rho^* (\nabla^* \cdot \boldsymbol{u}^*)) = 0,$$

$$\text{Momentum:} \qquad \rho^* \left(\frac{\partial \boldsymbol{u}^*}{\partial t^*} + \boldsymbol{u}^* \cdot \nabla^* \boldsymbol{u}^* \right) = -\nabla^* p^* + (\rho^* - 1)\hat{\boldsymbol{e}}_z, \tag{7}$$

$$\text{Energy:} \qquad \rho^* \left(\frac{\partial T^*}{\partial t^*} + \boldsymbol{u}^* \cdot \nabla^* T^* \right) = \dot{q}'''^*.$$

For future reference, also define the following characteristic quantities for the vorticity, ω, potential, Φ, and Stokes stream function, Ψ:

$$\omega_c = t_c^{-1} = \left(\frac{g^3 \rho_o c_p T_o}{\dot{Q}_o} \right)^{1/5}, \quad \Phi_c = L_c^2 t_c^{-1} = \left(\frac{g^{1/3} \dot{Q}_o}{\rho_o c_p T_o} \right)^{3/5}, \quad \text{and} \quad \Psi_c = L_c^3 t_c^{-1} = \frac{\dot{Q}_o}{\rho_o c_p T_o}. \tag{8}$$

Baum and McCaffrey [5] used these to describe any single fire by physically scaling McCaffrey's empirical vertical velocity and temperature profiles [9] resulting in

$$u^*_{z,e} = U^*_{cl}(z^*) exp\left\{ -\left(\frac{r^*}{R^*(z^*)} \right)^2 \right\}, \qquad \frac{(T - T_o)}{T_o} = \Theta^*_{cl}(z^*) exp\left\{ -\left(\frac{r^*}{\lambda R^*(z^*)} \right)^2 \right\}. \tag{9}$$

Three regions are defined: continuous flame, intermittent flame, and far field (see TABLE 1). $r = R(z)$ is the 1/e point of the Gaussian velocity profile. λ is the ratio of the thermal to the momentum radii. U^*_{cl} and Θ^*_{cl} are the averaged empirical center-line values which have the form $U^*_{cl} = A(z^*)^n$ and $\Theta^*_{cl} = B(z^*)^{2n-1}$. A, B, and n depend on the vertical flame region. For completeness, a fit for the width, $R^*_f = Ce^{-n^2 z^*} + D \cdot [z^*]^{3(1-2n)/5}$, based on the results of Eqs. (9) is included in TABLE 1 [8]. McCaffrey's data [9] suggest that $\lambda = 0.75^{1/2} = 0.866$.

TABLE 1. Baum and McCaffrey Plume Correlation Parameters

Region	Range	*n*	*A*	*B*	*C*	*D*
Flame	$0 \le z^* \le 1.32$	1/2	2.18	2.91	0	0.417
Intermittent	$1.32 \le z^* \le 3.3$	0	2.45	3.81	0.255	0.137
Plume	$z^* \ge 3.3$	-1/3	3.64	8.41	0.175	0.126

To obtain the radial velocities, the technique of flow field decomposition [5] is employed. The nondimensional flow field, $\boldsymbol{u}^*$, is described in axisymmetric cylindrical coordinates by the summation of an irrotational ($\nabla^* \times \boldsymbol{w}^* = \boldsymbol{0}$) expansion velocity, $\boldsymbol{w}^*$, governed by a potential, $\Phi^*(r^*, z^*)$, and a vorticity driven solenoidal ($\nabla^* \cdot \boldsymbol{v}^* = 0$) velocity, $\boldsymbol{v}^*$, described by a stream function, $\Psi^*(r^*, z^*)$, such that

$$u^*_r = \frac{\partial \Phi^*}{\partial r^*} - \frac{1}{r^*} \frac{\partial \Psi^*}{\partial z^*} \qquad \text{and} \qquad u^*_z = \frac{\partial \Phi^*}{\partial z^*} + \frac{1}{r^*} \frac{\partial \Psi^*}{\partial r^*}. \tag{10}$$

The details of obtaining u^*_r and u^*_z from Φ^* and Ψ^* based on Eqs. (6-10) are given in Refs. [5 and 8]. Once the nondimensional flow field for a single fire is known, the velocities induced by

N fires may be determined by simply scaling and summing. First, every fire is scaled using the heat release rate of the fire and atmospheric data as indicated in Eqs. (6). To find the velocities induced at any point (X_j, Y_j, Z_j), begin by calculating

$$\Delta X_{ij}^* = \frac{X_j - X_i}{L_{c_i}} \qquad \text{and} \qquad \Delta Y_{ij}^* = \frac{Y_j - Y_i}{L_{c_i}}, \tag{11}$$

where j indexes the calculation location within the flow field and i indexes the fires. ΔX_{ij}^* and ΔY_{ij}^* are the respective nondimensional distances from the fire at (X_i, Y_i). From these determine the nondimensional hypotenuse,

$$h_{ij}^* = \sqrt{(\Delta X_{ij}^*)^2 + (\Delta Y_{ij}^*)^2}. \tag{12}$$

Then calculate the X and Y velocity components induced at the j^{th} field point by the i^{th} fire,

$$U_{Xij}(Z_j) = U_{c_i}\left\{u_r^*(h_{ij}^*, z_j^*)\frac{\Delta X_{ij}^*}{h_{ij}^*}\right\} \quad \text{and} \quad U_{Yij}(Z_j) = U_{c_i}\left\{u_r^*(h_{ij}^*, z_j^*)\frac{\Delta Y_{ij}^*}{h_{ij}^*}\right\}, \tag{13}$$

since the cosine of the angle with the X-axis is $\Delta X_{ij}^*/h_{ij}^*$ and the sine is $\Delta Y_{ij}^*/h_{ij}^*$. Next, simply sum the velocity vectors at the desired point. Thus the non-axisymmetric velocity in the X-Y plane, $\boldsymbol{U}_H(X,Y,Z)$, can be derived by scaling and summing over each fire's axisymmetric u_r^*. To complete the three dimensional flow field, determine U_{Zij} as

$$U_{Zij}(Z_j) = U_{c_i}\left[u_z^*(h_{ij}^*, z_j^*)\right]. \tag{14}$$

Since, in general, h_{ij}^* will not fall directly on an (r^*, z^*) grid point, a bivariate modification of the polynomial interpolation routine POLINT [10] is used to determine the velocity at (h_{ij}^*, z_j^*).

Straight forward summation suffices to calculate the induced wind at all desired points:

$$U_X(X_j, Y_j, Z_j) = \sum_{i=1}^{N} U_{c_i}\left\{u_r^*(h_{ij}^*, z^*)\frac{\Delta X_{ij}^*}{h_{ij}^*}\right\}, \qquad U_Y(X_j, Y_j, Z_j) = \sum_{i=1}^{N} U_{c_i}\left\{u_r^*(h_{ij}^*, z^*)\frac{\Delta Y_{ij}^*}{h_{ij}^*}\right\},$$
$$U_Z(X_j, Y_j, Z_j) = \sum_{i=1}^{N} U_{c_i} u_z^*(h_{ij}^*, z^*), \tag{15}$$

where N is the total number of fires such that $1 \le i \le N$. Alternative methods to improve computation time by combining fires far from the point (X_i, Y_i, Z_i) and using asymptotic solutions are described in Ref. [8]. The accuracy of the mass fire velocity, $\boldsymbol{U}$, does not depend on the j-grid density.

RESULTS

The induced winds at early time for altitudes of 0 and 20 m were evaluated. No significant variation with altitude was observed. Limiting calculations to $Z \leq 30$ m ensures that plumes are independent. A technique for extending calculations to higher altitudes is described in Ref. [8]. In Figs. 3 and 4, the ambient, induced, and combined winds are represented by light gray, medium gray, and black vectors, respectively, at the center of each sector. The magnitude of the combined wind is given in m.p.h. in the corner opposite the arrow head in each sector. Below it is the angle, given in the meteorological convention, measured from the north direction to the tail of the combined wind vector. In Fig. 3, it is evident that thirty eight 50 MW fires do not induce much of a flow. The maximum induced velocity is 2.6 m/s. This indicates that no significant induced velocities occurred prior to 11:45 a.m. At noon, as is shown in Fig. 4, the 259 fires of various strengths now induce much higher velocities. Of note is the maximum induced speed of 13.4 m/s which is strong enough to noticeably affect local weather patterns.

Figure 4 indicates that the simple combination of a streaming atmospheric wind and the fire induced wind is characterized by an augmented flow towards the burning area from the upwind direction and a nearly stagnant flow on the lee side of the fire zone just downwind of the conflagration. It is evident that the fire's effect is to draw air in towards the over-all centroid of the fires. In Fig. 4, a comparison of the atmospheric and combined vectors demonstrates a small change in direction and a significant increase in magnitude for those vectors upwind of the fires. Downwind, the induced flow opposes the ambient flow, reversing its direction and substantially lowering its magnitude. It is believed that this phenomenon played a role in the rapid slowdown of the fire spread at noon [1], thereby demonstrating that, when a fire reaches conflagration proportions, its spread in the (atmospheric) windward direction may be curtailed by the flow induced into the mass fire plumes. This effect may need to be taken into account when planning conflagration combating strategies. Figure 6, also at noon, demonstrates a dramatic drop in horizontal velocity, $|\boldsymbol{U}_H|$, within the fire boundary, corresponding to a change from horizontal momentum to vertical momentum due to fire-produced buoyancy forces. At the fire perimeter, the field has its maxima and then decays smoothly in directions radially away from the mass fire center

Verification of large scale fire models is hampered by insufficient field data and the difficulty of conducting full scale experiments. No fire-induced wind data were formally collected for the Oakland Hills Fire. However, these results can be compared with the maximum velocities from various published large-scale fire tests. In the sixties, several scenarios were investigated under the auspices of Project Flambeau [11-13] in the western United States in order to quantify the effects of the massive fires as would be expected in nuclear attacks. Similar experiments were carried out in Australia [16] (Operation Euroka). More recently, large scale fire experiments were conducted in Canada [17] (Canadian Mass Fire Experiments). From TABLE

2, it can be seen that the induced flow speeds obtained in the present study (2.6 m/s at 11:45 a.m. and 13 m/s at noon) are consistent with the measured speeds reported in these mass fire experiments. The authors of Refs. [19 and 20] also applied the Baum and McCaffrey model to the Canadian Mass Fire Experiment. They were able to obtain good magnitude and encouraging directional agreement but found that the accuracy was dependent on how the mass fire was modeled as a collection of pool fires. The present authors observed similar behavior when they attempted a detailed comparison with Operation Euroka [8]. No unique solution emerged as the 6 Gg of dry brigalow (*Acacia Harpophylla*) arranged in 30 rows 460 m long were modeled as different numbers of axisymmetric sources. It appears that a line fire plume approach will be required to model Operation Euroka.

TABLE 2. Fire-Induced Wind Literature Comparison

Reference	Maximum Velocity (m/s)
Baum, H.R., and McCaffrey, B.J., Ref. [5]	10
Countryman, C.M., Ref. [14]	19
Countryman, C.M., Ref. [11]	11 - 22
Adams, J.S., Williams, D.W., and Tregellas-Williams, J., Ref. [16]	4 - 16
Palmer, T.Y., Ref. [15]	6 - 20
Pitts, W.M., Ref. [18]	15 - 40
Quintiere, J.G., Ref. [17]	12
Present Study, 11:45 AM	2.6
Present Study, 12:00 PM	13

CONCLUSIONS

The winds generated by the houses observed to be at peak burn at 11:45 a.m. and 12:00 p.m. for the Oakland Hills Fire were simulated using the Baum and McCaffrey mass fire model. For a single house burning at 50 MW, Eqs. (9) and TABLE 1 of the Baum and McCaffrey single plume model yield a maximum temperature of 1170 K; it occurs in the continuous flame zone. Furthermore, for this single house example the flame tip is 15 m high, the maximum vertical velocity is 16 m/s, and the maximum radial velocity is 2.4 m/s. The steady state mass fire model, as is shown in Eqs. (15), is based on superposition of individual plumes. At 11:45 a.m., with 38 sources at 50 MW, the maximum horizontal velocity is 13 m/s. The maximum vertical velocity is 14 m/s. At 12:00 a.m., with 259 sources at $\geq$ 50 MW, the maximum horizontal velocity is 13 m/s. The maximum vertical velocity is 26 m/s. It is believed that these strong fire-induced winds that occurred at and after 12:00 p.m. contributed to the post-noon slow down of the fire spread rate in the ambient wind direction. The flows induced at noon effectively negate the ambient wind downwind of the mass fire.

Although no direct comparisons with the Oakland Hills Fire are possible since no velocity data were recorded for this fire, the results presented are consistent with data published for other multiple source, mass fire experiments. However, this mass fire model cannot be used for

fuel configurations that cannot be identified as individual, nearly-symmetric sources, e.g., the Operation Euroka [16] fire which had its fuel arranged in 30 long rows.

ACKNOWLEDGMENTS

This paper is dedicated to Battalion Chief James M. Riley, Jr., and Police Officer John W. Grubensky who gave their lives rescuing victims of the Oakland Hills Conflagration. The authors appreciate support under grant No. 60NANB3D1438 from the Building and Fire Research Laboratory of the National Institute of Standards and Technology, U.S.D.O.C.

REFERENCES

1. Pagni, P. J., "Causes of the 20 October 1991 Oakland Hills Conflagration," Fire Safety Journal, 21:4, 331 - 340, 1993.
2. Silberman, Robin, and Staff of Oakland Fire Dept., The Oakland Tunnel Fire, October 20, 1991: A Comprehensive Report, Official Oakland Fire Dept. Report, Oakland, CA, Feb., 1992.
3. Fowler, D., editor, Response of the San Francisco Fire Department to the Oakland-Berkeley Conflagration of October 20 and 21, 1991, S.F. Fire Dept. Report, San Francisco, July, 1992.
4. Teague, P.E., and Staff of the N.F.P.A., The Oakland/Berkeley Hills Fire, October 20, 1991, Quincy, MA, National Fire Protection Association, 1993.
5. Baum, H.R., and McCaffrey, B.J., "Fire-Induced Flow Field - Theory and Experiment," Fire Safety Science - Proceedings of the 2nd Int'l Symposium, pp. 129 - 148, Hemisphere, New York, 1989.
6. Sapsis, D., and Martin, R., NSF Report on Oakland Hills Fire, to be published.
7. Monteverdi, J., personal communiqué.
8. Trelles, J., Mass Fire Modeling of the 20 October 1991 Oakland Hills Fire, Ph.D. Dissertation, University of California at Berkeley, 1995.
9. McCaffrey, B.J., "Momentum Implications for Buoyant Diffusion Flames," Comb. and Flame 52, 149 - 167, 1986.
10. Press, N.H., et al., *Numerical Recipes,* 2nd ed., Cambridge U. Press, Cambridge, England, 1992.
11. Countryman, C.M., "PROJECT FLAMBEAU - An Investigation of Mass Fires (1964-1967), Final Report - Volume I," Pacific Southwest Forest and Range Experiment Station, Berkeley, CA, 1969.
12. Palmer, T.Y., "PROJECT FLAMBEAU - An Investigation of Mass Fires (1964-1967), Final Report - Volume II: Catalogue of Project Flambeau Fires, 1964-1967," P.S.W. Forest and Range Experiment Station, Berkeley, CA, 1969.
13. Storey, T.G., et al., "PROJECT FLAMBEAU - An Investigation of Mass Fires (1964-1967), Final Report - Volume III: Appendixes, 1964-1967," P.S.W. Forest and Range Experiment Station, Berkeley, CA, 1969.
14. Countryman, C.M., "Mass Fires and Fire Behavior," PSW-19, Pacific Southwest Forest and Range Experiment Station, Berkeley, CA, 1964.
15. Palmer, T.Y., "Large Fire Winds, Gases and Smoke," Atmos. Env., 15:10/11, 2079 - 2090, 1981.
16. Adams, J.S., Williams, D.W., and Tregellas-Williams, J., "Air Velocity, Temperature, and Radiant-Heat Measurements within and around a Large Free-burning Fire," 14th Int'l Symposium on Combustion, pp. 1046 - 1049, The Combustion Institute, Pittsburgh, P.A., 1973.
17. Quintiere, J.G., "Canadian Mass Fire Experiment, 1989," J. of Fire Prot. Eng., 5:2, 67 - 78, 1993.
18. Pitts, W.M., "Winds Effects on Fires," Prog. in Energy and Comb. Sci., 17, 83 - 134, 1991.
19. Quintiere, J.G., Canadian Mass Fire Experiment, 1989, NISTIR 4444, Nov. 1990.
20. Ohlemiller, T., and Corley, D., "Heat Release Rate and Induced Wind Field in a Large Scale Fire," Comb. Sci. and Tech., 97, 315 - 330, 1994.